Journal of Sound and Vibration (2000) **233**(1), 63–80
doi:10.1006/jsvi.1999.2791, available online at http://www.idealibrary.com on IDEAL®

FINITE ELEMENT ANALYSIS OF THREE-DIMENSIONAL VIBRATIONS OF THICK CIRCULAR AND ANNULAR PLATES

C.-F. Liu* and Y.-T. Lee

Department of Mechanical Engineering, National Sun Yat-Sen University, Kaohsiung, Taiwan 804, *Republic of China*

(*Received* 8 *July* 1999, *and in final form* 17 *November* 1999)

Three-dimensional vibrations of thick circular and annular plates are analyzed by a finite element method which, with a properly assumed set of displacement field, is different from the traditional 3-D finite element analysis and is reduced to a sequence of 2-D analyses one for each circumferential wave number. The present approach has several unique features: (1) It can obtain vibration frequencies which are comparable to, or as accurate as, those by other three-dimensional approaches, whenever comparisons between them are possible, and yet the formulation of the present method is simpler and its application is straightforward. (2) Different simply supported boundary conditions can be exactly imposed with the present approach. The latter feature may be quite difficult, if not impossible, for other methods. In the present analysis, vibration frequencies of a circular and an annular plate under different combinations of boundary conditions, wave numbers and finite element meshes are calculated, vibration characteristics are examined, and some typical mode shapes are shown graphically. Then, the results of some example problems by the present method are compared to those available in the literature to show its validity and accuracy.

1. INTRODUCTION

There are numerous publications of vibrating circular and annular plates in the literature. However, only a relatively limited number of these deal with this problem with three-dimensional approaches and Leissa [1–3] and Hutchinson [4–6] are the two most notable ones. When vibrations of circular and annular plates are analyzed by the conventional two-dimensional (2-D) (plate) theories, some behaviors in the thickness direction cannot be taken into account and some boundary conditions are just impossible to impose exactly [7]. Therefore, the vibration frequencies obtained by 2-D methods may be overestimated or underestimated, and some vibration modes would never appear in the analysis [8]. As to 3-D analysis, a 3-D analytical solution based upon series consisting of Bessel functions in the radial co-ordinate and trigonometric functions in the circumferential and thickness co-ordinates was presented by Hutchinson [4] for the vibration analysis of thick, free circular plates. So and Leissa [3] proposed a 3-D Ritz method to solve similar types of problems, made comprehensive comparisons, and presented various vibration modes. However, due to the nature of their approaches, analysis of circular plates with simply supported boundary conditions might be a very tough job for them to do. In the present study, 3-D vibrations of circular and annular plates are analyzed with a finite element which is based on a properly assumed displacement field and is not a traditional, 3-D element. Therefore, we can obtain 3-D results without paying the cost of 3-D analysis

0022-460X/00/210063 + 18 $35.00/0

and also need not deal with its complicated output. Vibration frequencies of a circular and an annular plate under different combinations of boundary conditions, wave numbers, and finite element meshes are derived first, vibration characteristics are examined, and convergence is tested. Some typical mode shapes are drawn. Then, results by the present approach for some problems are compared with the other most accurate results known to date.

2. FORMULATION

The displacement field is assumed as

$$u = U(r, z, t)\cos n\theta, \qquad v = V(r, z, t)\sin n\theta, \qquad w = W(r, z, t)\cos n\theta, \tag{1}$$

where u, v, w are the displacements in the radial, circumferential, and thickness (axial) directions, respectively, r, θ, and z are the corresponding co-ordinates in these directions, $n = 0, 1, 2, \ldots, \infty$, representing the circumferential wave numbers, and t is time variable.

This is a displacement field that satisfies the 3-D elasticity equations of motion (of circular plates), expressed in cylindrical co-ordinates, when synchronous, sinusoidal motion is assumed. These are also the same displacements used in reference [3] and elsewhere.

The displacements are then substituted into the strain–displacement relations, and the strains are therefore expressed in terms of displacements. The stress–strain equations, in turn, lead to stresses which are also expressed in terms of displacements.

The finite element formulation of vibrating plates requires Hamilton's principle:

$$0 = \int_0^t \left[\int_{\text{vol}} [\sigma_r \delta\varepsilon_r + \sigma_z \delta\varepsilon_z + \sigma_\theta \delta\varepsilon_\theta + \tau_{z\theta}\delta\gamma_{z\theta} + \tau_{r\theta}\delta\gamma_{r\theta} + \tau_{rz}\delta\gamma_{rz}) - (\dot{u}\delta\dot{u} + \dot{v}\delta\dot{v} + \dot{w}\delta\dot{w})] \, \mathrm{d}V \right] \mathrm{d}t, \tag{2}$$

where $\dot{u}$, $\dot{v}$, and $\dot{w}$ are the velocity components in the three co-ordinate directions. After substituting stresses and strains obtained via strain–displacement and stress–strain relations into the above equation, we end up with a variational form where the three displacements are the only primary variables. The general practice of the finite element method is then followed. If the integration is carried out with respect to a single finite element, the element equation can be derived as

$$[m]\{\ddot{U}\} + [k]\{U\} = 0, \tag{3}$$

where $\{U\}^{\mathrm{T}} = [U_1, U_2, \ldots, U_m, V_1, V_2, \ldots, V_m, W_1, W_2, \ldots, W_m]$, m is the number of nodes in an element, and $[m]$ and $[k]$ are the elemental mass and stiffness matrices; see Appendix A.

The global equation of motion can be obtained by assembling all the element equations:

$$[M]\{\ddot{X}\} + [K]\{X\} = 0 \tag{4}$$

which corresponds to an eigenvalue equation of the following form:

$$[K]\{x\} = \lambda[M]\{x\}. \tag{5}$$

The eigenvalue λ denotes the square of vibration frequency ω and eigenvector $\{x\}$ represents the corresponding mode shape.

3. RESULTS AND DISCUSSIONS

To have a clearer understanding of the vibration of circular and annular plates under different boundary conditions, circumferential wave numbers (n), radial wave numbers (s) or modal numbers, and finite element meshes, numerical results are presented for a circular plate with $a/h = 5$ where a is the outer radius and h is the thickness of the plate and an annular plate with $a/h = 10$ and $b/a = 0{\cdot}5$ where b is the inner radius. Both plates have the Poisson ratio 0·3. The boundary conditions employed are completely free, clamped, ss1, ss2, ss3, and ss4 for the circular plate and completely free, c–f, ss1–f, ss3–f, c–c, ss1–ss1, and ss3–ss3 for the annular plate where "c" represents the clamped condition, and "f" denotes free boundary. The two conditions before and after the dash denote those at the inner and outer edges of an annular plate respectively. The four simply supported conditions are shown in Figure 1. In all cases, the finite element employed is an 8-node isoparametric 2-D element (in rz-plane). Therefore, for each value of n, the present analysis is reduced to a two-dimensional analysis and can save a lot of computer time. The finite element meshes are generated with equally spaced grids in both r and z directions. Frequency ω is non-dimensional according to $\bar{\omega} = \omega a\sqrt{(\rho/G)}$.

The finite element non-dimensional frequencies of a circular plate are listed in Table 1 for the axisymmetric case, $n = 0$. A superscript " $+$" denotes a radial straining mode, as seen in Figure 2, and a "*" denotes circumferentially vibrating mode, as seen in Figure 3. Values in Table 1 without any superscript represent flexural mode non-dimensional frequencies, as seen in Figure 4. These symbols will stand for the same things in this paper unless otherwise noted. From Table 1, we may find that:

(1) Radial straining modes or circumferentially vibrating modes exist in the first five modes regardless of the boundary conditions. The radial straining modes appear as the third one for the free, ss2, and ss4 cases and have almost the same frequency. The circumferentially vibrating modes occur as the fourth mode for the free boundary condition and at first the fourth mode and then the fifth mode (this is due to mesh refinement and the redistribution of the system stiffness and mass matrices which might follow) for ss2, and the fifth mode for ss4, also with the same $\bar{\omega}$. On the other hand, circumferentially vibrating modes appear as the third mode for the clamped, ss1, and ss3 cases and the radial straining modes as the fifth mode for the clamped and ss1 cases. However, their frequencies are not close to each other.

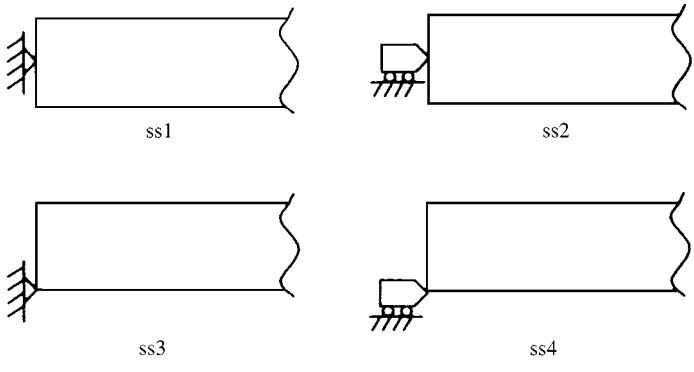

Figure 1. Simply supported boundary conditions.

TABLE 1

The first five non-dimensional frequencies $\bar{\omega}$'s of a circular plate for different boundary conditions and finite element meshes ($a/h = 5$, $v = 0{\cdot}3$ and $n = 0$)

BC	Mesh	Mode 1	2	3	4	5
Free	(5 × 2)	0·8319	3·074	3·457^{+}	5·137*	6·002
	(10 × 2)	0·8316	3·063	3·457^{+}	5·136*	5·198
	(20 × 2)	0·8316	3·062	3·457^{+}	5·136*	5·912
	(20 × 4)	0·8314	3·059	3·457^{+}	5·136*	5·900
Clamped	(5 × 2)	0·9187	3·036	3·832*	5·790	6·496^{+}
	(10 × 2)	0·9135	3·008	3·832*	5·682	6·487^{+}
	(20 × 2)	0·9115	3·001	3·832*	5·665	6·484^{+}
	(20 × 4)	0·9102	2·993	3·832*	5·644	6·482^{+}
ss1	(5 × 2)	0·4672	2·460	3·487*	5·232	5·504^{+}
	(10 × 2)	0·4668	2·447	3·391*	5·151	5·382^{+}
	(20 × 2)	0·4668	2·441	3·319*	5·123	5·283^{+}
	(20 × 4)	0·4663	2·432	3·247*	5·085	5·139^{+}
ss2	(5 × 2)	0·4672	2·460	3·457^{+}	5·138*	5·232
	(10 × 2)	0·4668	2·447	3·457^{+}	5·136*	5·151
	(20 × 2)	0·4668	2·441	3·457^{+}	5·123	5·136*
	(20 × 4)	0·4663	2·432	3·457^{+}	5·085	5·136*
ss3	(5 × 2)	0·6770	2·537	2·875*	4·391^{p}	5·515^{p}
	(10 × 2)	0·6675	2·505	2·759*	4·284^{p}	5·306^{p}
	(20 × 2)	0·6618	2·483	2·663*	4·243^{p}	5·147^{p}
	(20 × 4)	0·6504	2·462	2·567*	4·141^{p}	5·007^{p}
ss4	(5 × 2)	0·4629	2·382	3·457^{+}	4·881	5·138*
	(10 × 2)	0·4615	2·343	3·456^{+}	4·695	5·136*
	(20 × 2)	0·4607	2·322	3·456^{+}	4·602	5·136*
	(20 × 4)	0·4596	2·291	3·456^{+}	4·469	5·136*

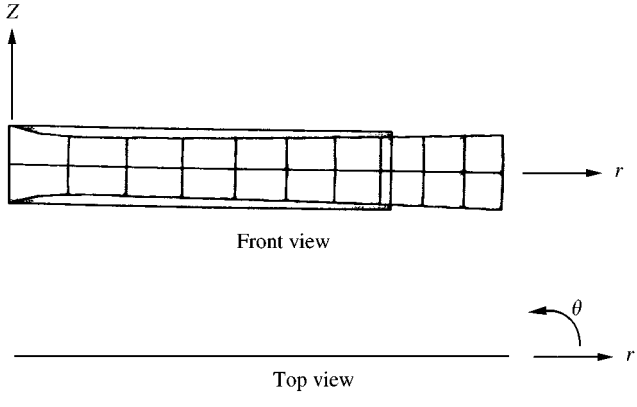

Figure 2. A typical radial straining mode (Table 1. free, $n = 0$, mode = 3).

(2) Flexural modes for ss1 and ss2 have the same non-dimensional frequencies which are different from those of ss3 and ss4. ss3 is especially different from the other three simply supported cases in many aspects.

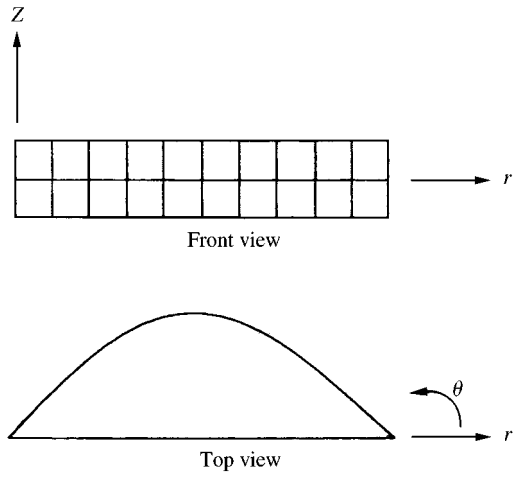

Figure 3. A typical circumferentially vibrating mode (Table 1. clamped, $n = 0$, mode = 3).

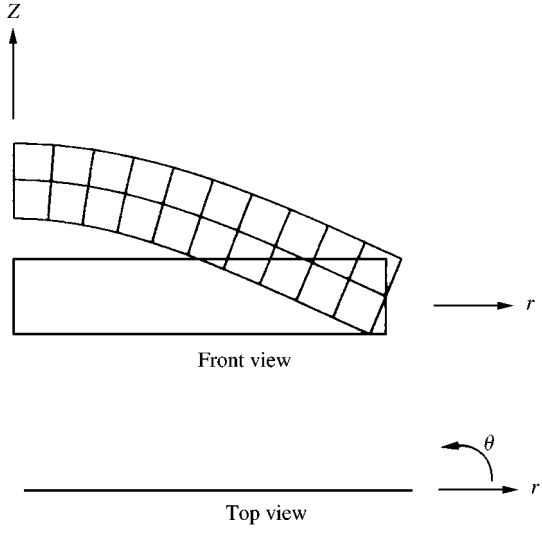

Figure 4. A typical flexural mode (Table 1. ss1, $n = 0$, mode = 1).

From 1 and 2 above, we may conclude that the boundary effect on $\bar{\omega}$ is different for different types of vibration modes. The fact that the free, ss2, and s4 cases all have the same in-plane modes with the same frequencies may be attributed to the non-restraining of the in-plane displacements at boundaries, though the transverse displacement conditions are specified in different ways. Also, in this case, the first in-plane mode is a radial straining mode. When there is radial constraint (clamped, ss1 and ss3), the first in-plane mode is of a circumferentially vibrating type, instead. As to the flexural modes, on the contrary, the same transverse displacement conditions specified at symmetric location lead to the same $\bar{\omega}$ whether there is in-plane constraint at boundary or not.

(3) Convergence of the non-dimensional frequencies along with the finite element mesh refinements for all the cases in Table 1 are monotonic. However, the convergence rate

for different mode types and boundary conditions may be different. Both the in-plane modes mentioned in (1) have very quick convergence for the free, clamped, ss2 and ss4 cases no matter what their modal numbers are. When only the boundary conditions are concerned, convergence of the free and the clamped cases are, in general, better than other types of boundary conditions. ss3 has the slowest and worst convergence among all, *but still it is not too bad* (the difference between 20×20 and 20×4 is $< 2{\cdot}5\%$).

(4) Frequencies for the simply supported condition are lower than for clamped cases as usual. However, it is interesting to find from Table 1 that the fundamental frequency of the free case is higher than those of the four simply supported conditions, and the second and the third axisymmetric flexural modes of the free cases are the highest among all the boundary conditions.

It should also be noted that, if we look at the displacements, the mode shown in Figure 3 should not appear for $n = 0$. So and Leissa [3] use a complementary set of functions which replace $\cos n\theta$ by $\sin n\theta$, and conversely, to obtain this type of mode. However, either set of displacements will lead to the same system equation with our formulation when $n = 0$, none of the modes is missing, and this might be another advantage of the present method.

Table 2 shows the non-dimensional frequencies of the same circular plate as in Table 1 with $n = 1$. A superscript "s" denotes that it is a radial straining mode at $\theta = 0$ and a circumferentially vibrating mode at $\theta = 90$, and so it is an in-plane mode without transverse displacement w; see Figure 5. As to "p", it is a combination of different vibration modes, as in Figure 6. Compared to Table 1, we may find that the observations from Table 1 would not totally apply to cases with $n = 1$. From Table 2, flexural modes of ss1 (the 1st and the 3rd modes) still resemble those of ss2 (the 2nd and the 4th modes) and have the same frequencies, and the explanation we give for the same situation in Table 1 is applicable here as well. The first in-plane mode of ss2 has exactly the same frequency as ss4, with almost the same mode shape. But, the third mode of ss2 has a different mode shape from that of ss4, in spite of the close $\bar{\omega}$'s of the two; see Figure 6. Convergence is also monotonic for all cases and the free case still has the fastest convergence as for $n = 0$. In-plane modes (with superscript "s") in general have better convergence for free, clamped, and ss2 (difference of $\bar{\omega}$'s between 20×2 and $20 \times 4 < 0{\cdot}1\%$). That in-plane modes of free, ss2 and ss4 do not have the same $\bar{\omega}$'s as in Table 1 may be due to the non-axisymmetry for $n = 1$. It is also noteworthy that the lowest mode is an in-plane mode, and not a flexural mode for this case of $n = 1$.

Tables 3–6 list the non-dimensional frequencies for $n = 0$–3, $s = 1$–5, with different boundary conditions (f–f, c–f, s1–f, s3–f, c–c, s1–s1, s3–s3) and finite element meshes (5×2, 10×2, 20×2, 20×4). A superscript "a" means that the mode is of an antisymmetric type ($u(z) = -u(-z)$, $v(z) = -v(-z)$, $w(z) = w(-z)$), as seen in Figure 7, which is different from the symmetric modes ($u(z) = u(-z)$, $v(z) = v(-z)$, $w(z) = -w(z)$) with superscript " + " or "*" or "s". Since f–f cases always have fast convergence, only 5×2 and 10×2 meshes are used.

These results reveal the complex nature of the vibration of annular plates. Some observations that might not be familiar to the reader are listed below.

(1) Fundamental frequencies (flexural modes) for the f–f cases are not necessarily lower for smaller n, e.g., $\bar{\omega}_1$'s for $n = 2$ and 3 are smaller than for $n = 1$. However, for the other types of boundary conditions, $\bar{\omega}_1$ increases monotonically with the increasing of n.

(2) Non-dimensional fundamental frequencies with $n = 0$ and 1 for the f–f condition are larger than those for s1–f and s3–f. This is similar to what we have found for the

TABLE 2

The first five non-dimensional frequencies $\bar{\omega}$'s of a circular plate for different boundary conditions and finite element meshes ($a/h = 5$, $\nu = 0{\cdot}3$ and $n = 1$)

BC	Mesh	Mode 1	2	3	4	5
Free	(5 × 2)	1·765	2·733[s]	4·420	5·945[s]	6·842[s]
	(10 × 2)	1·763	2·733[s]	4·391	5·944[s]	6·835[s]
	(20 × 2)	1·763	2·733[s]	4·388	5·944[s]	6·835[s]
	(20 × 4)	1·762	2·733[s]	4·382	5·944[s]	6·835[s]
Clamped	(5 × 2)	1·844	3·792[s]	4·369	5·645[s]	7·383
	(10 × 2)	1·811	3·725[s]	4·287	5·595[s]	7·142
	(20 × 2)	1·797	3·675[s]	4·264	5·561[s]	7·102
	(20 × 4)	1·793	3·674[s]	4·250	5·561[s]	7·071
ss1	(5 × 2)	1·298	3·214[s]	3·797	5·136[s]	6·829
	(10 × 2)	1·278	3·077[s]	3·735	4·969[s]	6·627
	(20 × 2)	1·267	2·968[s]	3·708	4·849[s]	6·565
	(20 × 4)	1·264	2·871[s]	3·687	4·760[s]	6·501
ss2	(5 × 2)	0·8595[s]	1·298	2·938[s]	3·797	6·388[s]
	(10 × 2)	0·7973[s]	1·278	2·906[s]	3·735	6·336[s]
	(20 × 2)	0·7470[s]	1·268	2·883[s]	3·708	6·293[s]
	(20 × 4)	0·7467[s]	1·264	2·883[s]	3·686	6·292[s]
ss3	(5 × 2)	1·340[p]	2·544[p]	3·953[p]	4·430[p]	6·261[p]
	(10 × 2)	1·304[p]	2·417[p]	3·826[p]	4·282[p]	5·955[p]
	(20 × 2)	1·280[p]	2·338[p]	3·738[p]	4·169[p]	5·799[p]
	(20 × 4)	1·271[p]	2·246[p]	3·664[p]	4·083[p]	5·627[p]
ss4	(5 × 2)	0·8595[s]	1·272	2·937[p]	3·612	6·200
	(10 × 2)	0·7973[s]	1·244	2·904[p]	3·492	5·874
	(20 × 2)	0·7470[s]	1·229	2·881[p]	3·431	5·732
	(20 × 4)	0·7467[s]	1·220	2·881[p]	3·356	5·555

circular plate. However, for $n = 2$ and 3, $\bar{\omega}_1$'s of f–f are the lowest compared to those with the other boundary conditions.

(3) An in-plane mode plus one of the f–f, c–f, and c–c conditions guarantees a good, and mostly quick, convergence regardless of the values of n and modal number. Also, the completely free boundary condition is the only one that can have a general, faster convergence than the other boundary conditions, just the same as for circular plates.

4. COMPARISONS WITH OTHER RESULTS

To set up the validation of the present method and to check its accuracy, comparisons of the results for some typical problems by the present method with those known to be the most accurate are made. The finite element meshes employed, according to the convergence characteristics shown in Tables 1–6, will consist of finite elements, square in shape mostly with the side lengths of the element being $h/2$, $h/4$ and $h/8$ for $a/h = 5$ and 10, 2·5 and 1 when boundary condition is completely free. For problems with other boundary conditions, meshes will be specified otherwise.

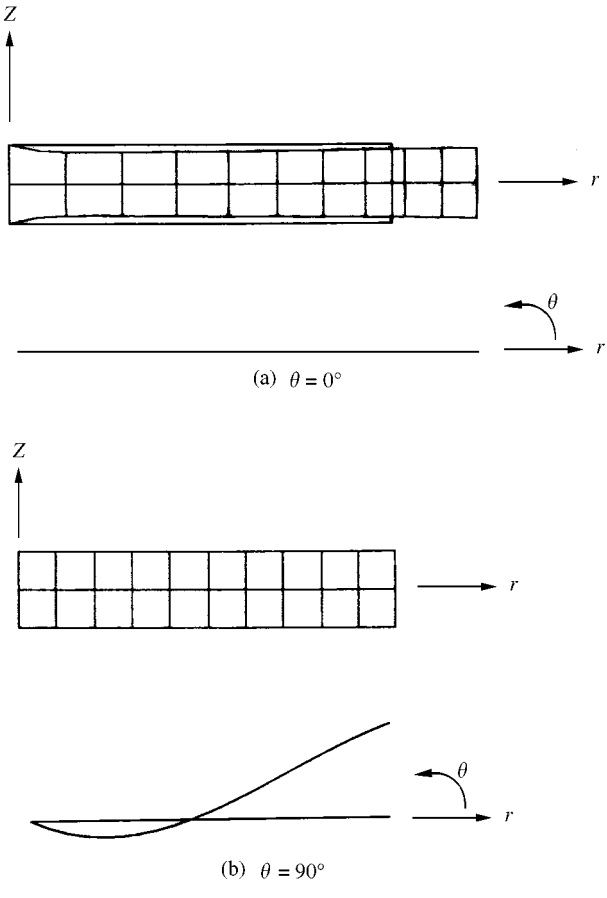

Figure 5. An in-plane mode which is a radial straining mode at $\theta = 0^\circ$ and a circumferentially vibrating mode at $\theta = 90^\circ$ (Table 5. c–f, $n = 2$, mode = 4).

Table 7 shows the non-dimensional flexural vibration frequencies of circular plates with $a/h = 10$ and 5. Boundary condition is completely free. The results of a 3-D Ritz method [3] and a 2-D Mindlin theory [9] are also listed. It is observed that very good agreement between the present results and those of the 3-D Ritz method has been achieved. Their difference of $\bar{\omega}$ is smaller than 0·5% for all cases of $a/h = 10$ and for most cases of $a/h = 5$, with the present results being a little higher. 2-D theory derives the lowest frequencies among the three methods. This is quite different from the traditional expectation that 2-D frequencies of plates are higher than those of 3-D.

Table 8 compares the non-dimensional flexural vibration frequencies of two annular plates with completely free edges among the 3-D Ritz method [4], the 3-D series method [6], the 2-D Mindlin theory [6], and the present method. The outer radius to thickness ratios (a/h) are 2·5 and 1, both with a ratio of inner to outer radius (b/a) equal to 0·5; hence, they are quite thick plates. It is amazing that the differences between the 3-D Ritz and the present one are smaller than 0·1% for all the cases expect two ($a/h = 2{\cdot}5$, $n = 0$, $s = 4$ and $a/h = 1$, $n = 0$, $s = 3$). Compared to the present results, some of Hutchinson's are overestimated and some underestimated, with small discrepancies for most of the cases. As to the Mindlin theory, it is not expected that a 2-D theory would obtain good results for

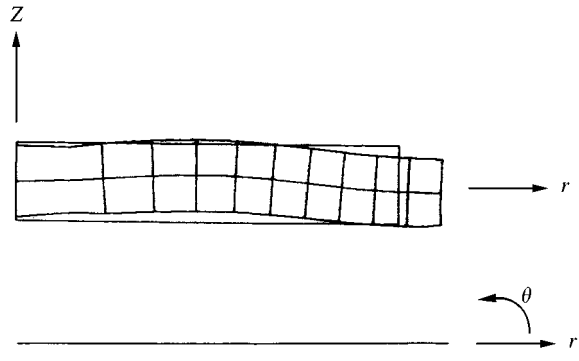

(a) $\theta = 0°$

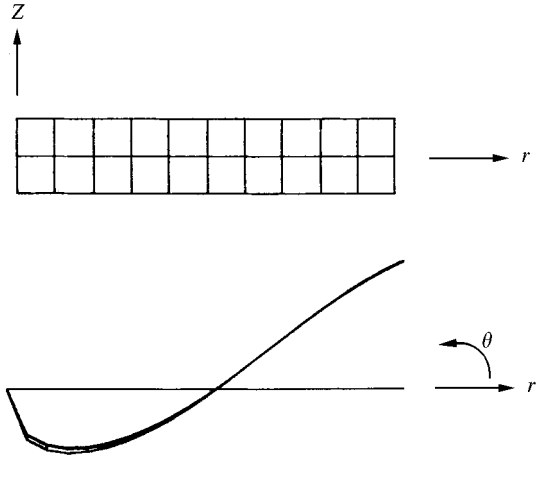

(b) $\theta = 90°$

Figure 6. A mixture of different vibration modes (Table 2. ss4, $n = 1$, mode = 3).

thick plates like these. The 2-D frequencies are always higher than the 3-D approaches, with the case $a/h = 2{\cdot}5$, $n = 0$, $s = 4$ being the only exception. Also, it is found that differences between 2-D and the present one are generally quite obvious for $s = 3$ and 4 of all cases with $a/h = 1$, and the worst ones are surprisingly those of $n = 0$, the axisymmetric cases.

Table 9 shows the comparisons of flexural vibration frequencies of an annular plate with $a/h = 1{\cdot}7$, $b/a = 0{\cdot}1765$ and completely free boundary conditions from the 3-D Ritz [3], a 3-D toroidal element [10] and the present. The present results are a little higher (difference $< 0{\cdot}5\%$) than those of the 3-D Ritz's as before and lower (difference $< 0{\cdot}5\%$) than those of reference [10].

Comparison of the non-dimensional flexural vibration frequencies of solid rods, fixed at one end and free at the outer circumferential surface and the other end, is demonstrated in Table 10 where L is the length of the rod and D is the diameter. Very good agreement is found between the present solutions and those of So [11].

Table 11 compares the four lowest $\bar{\omega}$'s of axisymmetric flexural modes for clamped circular plates with $a/h = 5$ and 2·5. The difference between the present solutions and those by 3-D series solutions of elasticity [12] is small ($< 0{\cdot}3\%$) for all the cases. Mindlin theory

TABLE 3

The first five non-dimensional frequencies $\bar{\omega}$'s of an annular plate for different boundary conditions and finite element meshes ($a/h = 10$, $b/a = 0{\cdot}5$, $\nu = 0{\cdot}3$ and $n = 0$)

n	Mode	Mesh	f–f	c–f	s1–f	s3–f	c–c	s1–s1	s3–s3
	1	(5 × 2)	0·4442	0·6236	0·1995	0·3386	3·569	1·823	2·583
		(10 × 2)	0·4442	0·6197	0·1995	0·3347	3·520	1·817	2·527
		(20 × 2)		0·6182	0·1995	0·3325	3·504	1·812	2·486
		(20 × 4)		0·6173	0·1995	0·3279	3·492	1·807	2·435
	2	(5 × 2)	$2{\cdot}237^{+}$	1·973*	1·746*	1·457*	6·394*	5·541*	4·475*
		(10 × 2)	$2{\cdot}236^{+}$	1·973*	1·687*	1·395*	6·393*	5·336*	4·278*
		(20 × 2)		1·973*	1·645*	1·345*	6·393*	5·191*	4·118*
		(20 × 4)		1·973*	1·605*	1·296*	6·393*	5·053*	3·963*
0	3	(5 × 2)	$3{\cdot}979^{a}$	$3{\cdot}482^{a}$	$2{\cdot}695^{a}$	$2{\cdot}543^{p}$	8·220	$6{\cdot}251^{a}$	$4{\cdot}545^{p}$
		(10 × 2)	$3{\cdot}970^{a}$	$3{\cdot}452^{a}$	$2{\cdot}685^{a}$	$2{\cdot}511^{p}$	8·052	$6{\cdot}167^{a}$	$4{\cdot}359^{p}$
		(20 × 2)		$3{\cdot}443^{a}$	$2{\cdot}679^{a}$	$2{\cdot}494^{p}$	8·014	6·124	$4{\cdot}278^{p}$
		(20 × 4)		3·436	2·671	$2{\cdot}469^{p}$	7·978	6·071	$4{\cdot}102^{p}$
	4	(5 × 2)	6·815*	$5{\cdot}411^{+}$	$4{\cdot}682^{+}$	$4{\cdot}419^{p}$	$10{\cdot}93^{+}$	$8{\cdot}169^{+}$	$8{\cdot}097^{p}$
		(10 × 2)	6·814*	$5{\cdot}406^{+}$	$4{\cdot}576^{+}$	$4{\cdot}029^{p}$	$10{\cdot}90^{+}$	$7{\cdot}843^{+}$	$7{\cdot}718^{p}$
		(20 × 2)		$5{\cdot}402^{+}$	$4{\cdot}490^{+}$	$3{\cdot}961^{p}$	$10{\cdot}89^{+}$	$7{\cdot}588^{+}$	$7{\cdot}440^{p}$
		(20 × 4)		$5{\cdot}402^{+}$	$4{\cdot}365^{+}$	$3{\cdot}842^{p}$	$10{\cdot}89^{+}$	$7{\cdot}227^{+}$	$7{\cdot}162^{p}$
	5	(5 × 2)	$9{\cdot}200^{a}$	$8{\cdot}554^{a}$	$7{\cdot}593^{a}$	$7{\cdot}666^{p}$	12·64*	10·96*	9·279*
		(10 × 2)	$9{\cdot}098^{a}$	$8{\cdot}417^{a}$	$7{\cdot}495^{a}$	$7{\cdot}436^{p}$	12·63*	10·59*	9·035*
		(20 × 2)		$8{\cdot}393^{a}$	$7{\cdot}461^{a}$	$7{\cdot}285^{p}$	12·62*	10·35*	8·850*
		(20 × 4)		$8{\cdot}368^{a}$	$7{\cdot}412^{a}$	$7{\cdot}148^{p}$	12·62*	10·13*	8·680*

TABLE 4

The first five non-dimensional frequencies $\bar{\omega}$'s of an annular plate for different boundary conditions and finite element meshes ($a/h = 10$, $b/a = 0{\cdot}5$, $\nu = 0{\cdot}3$ and $n = 1$)

n	Mode	Mesh	f–f	c–f	s1–f	s3–f	c–c	s1–s1	s3–s3
	1	(5 × 2)	0·7722	0·6309	0·2197	0·3229	3·599	1·884	2·608
		(10 × 2)	0·7705	0·6265	0·2190	0·3166	3·551	1·876	2·553
		(20 × 2)		0·6251	0·2189	0·3122	3·535	1·872	2·512
		(20 × 4)		0·6246	0·2187	0·3070	3·523	1·866	2·462
	2	(5 × 2)	$2{\cdot}810^{s}$	2·611*	2·425*	$2{\cdot}029^{p}$	6·721*	5·846*	$4{\cdot}214^{p}$
		(10 × 2)	$2{\cdot}810^{s}$	2·611*	2·376*	$1{\cdot}958^{p}$	6·720*	5·643*	$4{\cdot}007^{p}$
		(20 × 2)		2·611*	2·340*	$1{\cdot}909^{p}$	6·719*	5·497*	$3{\cdot}892^{p}$
		(20 × 4)		2·611*	2·304*	$1{\cdot}846^{p}$	6·719*	5·346*	$3{\cdot}699^{p}$
1	3	(5 × 2)	$4{\cdot}101^{a}$	$3{\cdot}541^{a}$	$2{\cdot}772^{a}$	$2{\cdot}746^{p}$	8·258	$6{\cdot}303^{a}$	$5{\cdot}244^{p}$
		(10 × 2)	$4{\cdot}091^{a}$	$3{\cdot}511^{a}$	$2{\cdot}760^{a}$	$2{\cdot}723^{p}$	8·092	$6{\cdot}218^{a}$	$5{\cdot}067^{p}$
		(20 × 2)		$3{\cdot}503^{a}$	$2{\cdot}754^{a}$	$2{\cdot}710^{p}$	8·054	6·174	$4{\cdot}945^{p}$
		(20 × 4)		$3{\cdot}495^{a}$	$2{\cdot}746^{a}$	$2{\cdot}694^{p}$	8·018	6·121	$4{\cdot}805^{p}$
	4	(5 × 2)	$7{\cdot}401^{s}$	$5{\cdot}382^{+}$	4·689	$4{\cdot}181^{p}$	$10{\cdot}81^{s}$	$8{\cdot}212^{+}$	$8{\cdot}038^{p}$
		(10 × 2)	$7{\cdot}401^{s}$	$5{\cdot}377^{+}$	4·584	$4{\cdot}069^{p}$	$10{\cdot}79^{s}$	$7{\cdot}887^{+}$	$7{\cdot}670^{p}$
		(20 × 2)		$5{\cdot}377^{+}$	4·501	$4{\cdot}004^{p}$	$10{\cdot}78^{s}$	$7{\cdot}637^{+}$	$7{\cdot}397^{p}$
		(20 × 4)		$5{\cdot}372^{+}$	4·385	$3{\cdot}896^{p}$	$10{\cdot}77^{s}$	$7{\cdot}301^{s}$	$7{\cdot}130^{p}$
	5	(5 × 2)	$9{\cdot}277^{a}$	$8{\cdot}603^{a}$	$7{\cdot}651^{a}$	$7{\cdot}685^{p}$	13·02*	11·26*	9·689*
		(10 × 2)	$9{\cdot}174^{a}$	$8{\cdot}466^{a}$	$7{\cdot}549^{a}$	$7{\cdot}461^{p}$	13·00*	10·91*	9·443*
		(20 × 2)		$8{\cdot}442^{a}$	$7{\cdot}514^{a}$	$7{\cdot}314^{p}$	13·00*	10·68*	$9{\cdot}261^{p}$
		(20 × 4)		$8{\cdot}417^{a}$	$7{\cdot}471^{a}$	$7{\cdot}178^{p}$	13·00*	10·46*	$9{\cdot}055^{p}$

TABLE 5

The first five non-dimensional frequencies $\bar{\omega}$'s of an annular plate for different boundary conditions and finite element meshes ($a/h = 10$, $b/a = 0{\cdot}5$, $\nu = 0{\cdot}3$ and $n = 2$)

n	Mode	Mesh	f–f	c–f	s1–f	s3–f	c–c	s1–s1	s3–s3
	1	(5 × 2)	0·2038	0·6841	0·3497	0·4242	3·699	2·074	2·715
		(10 × 2)	0·2037	0·6802	0·3482	0·4184	3·652	2·064	2·663
		(20 × 2)		0·6783	0·3478	0·4146	3·636	2·059	2·622
		(20 × 4)		0·6777	0·3473	0·4107	3·624	2·051	2·575
	2	(5 × 2)	0·9483^{s}	3·720^{a}	3·000^{a}	2·541^{p}	7·595*	6·461^{a}	4·320^{p}
		(10 × 2)	0·9481^{s}	3·691^{a}	2·987^{a}	2·463^{p}	7·592*	6·374^{a}	4·107^{p}
		(20 × 2)		3·683^{a}	2·980^{a}	2·417^{p}	7·591*	6·329^{a}	4·000^{p}
		(20 × 4)		3·675	2·971^{a}	2·349^{p}	7·590*	6·273	3·800^{p}
2	3	(5 × 2)	1·376	3·808^{s}	3·564^{s}	3·543^{p}	8·376	6·598^{s}	6·320^{p}
		(10 × 2)	1·372	3·807^{s}	3·498^{s}	3·488^{p}	8·213	6·388^{s}	6·160^{p}
		(20 × 2)		3·807^{s}	3·446^{s}	3·446^{p}	8·176	6·227^{s}	6·034^{p}
		(20 × 4)		3·807^{s}	3·384^{s}	3·396^{p}	8·140	6·027^{s}	5·907^{p}
	4	(5 × 2)	4·192^{s}	5·533^{s}	5·021^{s}	4·655^{p}	10·70^{s}	8·462^{s}	8·052^{p}
		(10 × 2)	4·191^{s}	5·528^{s}	4·948^{s}	4·594^{p}	10·68^{s}	8·157^{s}	7·701^{p}
		(20 × 2)		5·524^{s}	4·894^{s}	4·562^{p}	10·67^{s}	7·935^{s}	7·440^{p}
		(20 × 4)		5·524^{s}	4·824^{s}	4·510^{p}	10·67^{s}	7·671^{s}	7·188^{p}
	5	(5 × 2)	4·454^{a}	8·744^{a}	7·817^{a}	7·812^{p}	13·92^{a}	12·07^{s}	10·48^{p}
		(10 × 2)	4·441^{a}	8·612^{a}	7·719^{a}	7·588^{p}	13·60^{a}	11·76^{s}	9·933^{p}
		(20 × 2)		8·588^{a}	7·680^{a}	7·451^{p}	13·52^{a}	11·55^{s}	9·627^{p}
		(20 × 4)		8·562^{a}	7·632^{a}	7·314^{p}	13·45^{a}	11·34^{s}	9·266^{p}

TABLE 6

The first five non-dimensional frequencies $\bar{\omega}$'s of an annular plate for different boundary conditions and finite element meshes ($a/h = 10$, $b/a = 0{\cdot}5$, $\nu = 0{\cdot}3$ and $n = 3$)

n	Mode	Mesh	f–f	c–f	s1–f	s3–f	c–c	s1–s1	s3–s3
	1	(5 × 2)	0·5403	0·8505	0·6304	0·6909	3·889	2·407	2·945
		(10 × 2)	0·5399	0·8466	0·6285	0·6865	3·844	2·395	2·894
		(20 × 2)		0·8456	0·6280	0·6841	3·829	2·387	2·854
		(20 × 4)		0·8446	0·6270	0·6812	3·817	2·378	2·811
	2	(5 × 2)	2·080	4·022^{a}	3·378^{a}	3·102^{p}	8·579	6·730^{a}	4·772^{p}
		(10 × 2)	2·076	3·994^{a}	3·362^{a}	3·042^{p}	8·421	6·641^{a}	4·567^{p}
		(20 × 2)		3·987^{a}	3·354^{a}	3·010^{p}	8·385	6·593^{a}	4·471^{p}
		(20 × 4)		3·979	3·343^{a}	2·965^{p}	8·349	6·534	4·288^{p}
3	3	(5 × 2)	2·247^{s}	4·732^{s}	4·353^{s}	4·128^{p}	8·777^{s}	7·462^{s}	7·530^{p}
		(10 × 2)	2·246^{s}	4·730^{s}	4·267^{s}	4·045^{p}	8·770^{s}	7·216^{s}	7·327^{p}
		(20 × 2)		4·730^{s}	4·203^{s}	3·987^{p}	8·768^{s}	7·024^{s}	7·162^{p}
		(20 × 4)		4·729^{s}	4·124^{s}	3·911^{p}	8·767^{s}	6·764^{s}	6·988^{p}
	4	(5 × 2)	5·004^{a}	6·353^{s}	6·129^{s}	5·938^{p}	10·83^{s}	9·121^{s}	8·301^{p}
		(10 × 2)	4·987^{a}	6·353^{s}	6·099^{s}	5·914^{p}	10·81^{s}	8·872^{s}	8·000^{p}
		(20 × 2)		6·348^{s}	6·080^{s}	5·904^{p}	10·81^{s}	8·700^{s}	7·791^{p}
		(20 × 4)		6·348^{s}	6·051^{s}	5·880^{p}	10·81^{s}	8·519^{s}	7·595^{p}
	5	(5 × 2)	5.749^{s}	8.983^{a}	8.100^{a}	8·056^{p}	14·28^{a}	12·35^{a}	10·76^{p}
		(10 × 2)	5·749^{s}	8·856^{a}	7·998^{a}	7·841^{p}	13·78^{a}	11·99^{a}	10·18^{p}
		(20 × 2)		8·832^{a}	7·958^{a}	7·710^{p}	13·71^{a}	11·84^{a}	9·865^{p}
		(20 × 4)		8·807^{a}	7·910^{a}	7·583^{p}	13·64^{a}	11·67^{a}	9·509^{p}

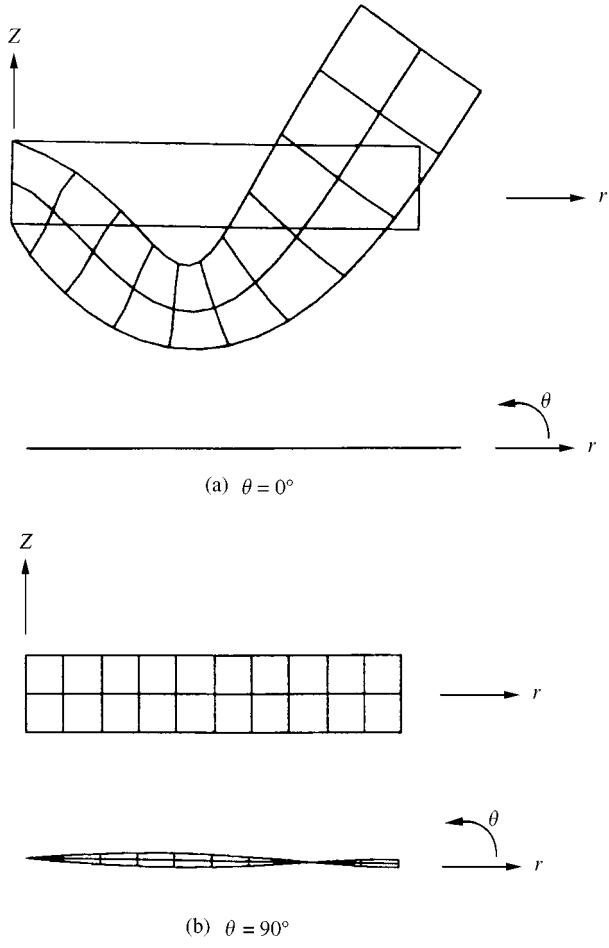

Figure 7. A typical antisymmetric vibration mode (Table 4. c–f, $n = 1$, mode = 3).

solutions obtained in reference [12] are also shown in Table 11 and are smaller than 3-D results, beyond expectation.

5. CONCLUDING REMARKS

In the present study, 3-D axisymmetric and non-axisymmetric vibrations of a circular and an annular plate are analyzed with various combinations of boundary conditions, wave numbers or modal numbers, and finite element meshes. Characteristics of the vibration are examined, different modes are separated and typical ones are demonstrated in graphs, and convergence with finite element mesh refinement is checked. From the results, several conclusions have been drawn and can help understand the vibration phenomena of circular and annular plates better. Convergence is monotonic for all cases. It means that convergence can always be reached by element mesh refinement even if the present numerical results of some cases might not be convergent to a satisfactory extent (which is limited by the resource available). However, for some cases, e.g., the completely free ones, convergence is quite good even with coarse meshes.

TABLE 7

Comparison of non-dimensional flexural vibration frequencies $\bar{\omega}$'s of circular plates between the present, the 3-D Ritz and the 2-D Mindlin theories, with $a/h = 10$ (mesh 20×2) and $a/h = 5$ (mesh 10×2)

		$a/h = 10$			$a/h = 5$		
n	s	Present	3-D Ritz	2-D	Present	3-D Ritz	2-D
0	1	0·4329	0·4329	0·4327	0·8316	0·8314	0·8300
	2	1·764	1·763	1·759	3·063	3·059	3·036
	3	3·765	3·761	3·741	5·918	5·898	5·821
	4	6·223	6·214	6·162	9·008	8·948	8·789
1	1	0·9633	0·9631	0·9618	1·763	1·762	1·754
	2	2·659	2·658	2·6747	4·391	4·381	4·336
	3	4·915	4·910	4·876	7·402	7·369	7·254
	4	7·542	7·532	7·453	10·55	10·463	10·250
2	1	0·2576	0·2576	0·2575	0·4997	0·4995	0·4991
	2	1·616	1·616	1·612	2·820	2·817	2·2798
	3	3·626	3·623	3·605	5·722	5·706	5·633
	4	6·098	6·090	6·039	z8·845	8·795	8·640
3	1	0·5892	0·5891	0·5887	1·107	1·106	1·104
	2	2·362	2·361	2·353	3·942	3·936	3·900
	3	4·647	4·643	4·613	7·045	7·020	6·915
	4	7·304	7·293	7·221	10·25	1·0179	9·981
4	1	1·017	1·016	1·015	1·844	1·843	1·863
	2	3·183	3·181	3·166	5·099	5·088	5·030
	3	5·709	5·702	5·658	8·353	8·318	8·178
	4	8·524	8·513	8·415	11·61	11·524	11·278
5	1	1·529	1·529	1·526	2·677	2·673	2·660
	2	4·063	4·059	4·036	6·272	6·255	6·173
	3	6·802	6·793	6·731	9·643	9·595	9·419
	4	9·755	9·743	9·615	12·92	12·823	12·533
6	1	2·117	2·116	2·111	3·577	3·570	3·547
	2	4·991	4·985	4·952	7·452	7·427	7·317
	3	7·918	7·907	7·825	10·91	10·850	10·636
	4	10·99	10·985	10·819	14·19	14·069	13·741

Typical example problems are also solved with the present method. The results are compared with those from the 3-D Ritz method, the 3-D series method, the 2-D Mindlin theory, and a 3-D toroidal finite element which are considered to be most accurate in the literature. Most of the examples feature completely free cases. One of the two exceptions is circular cylinders with one end fixed and the other surfaces free. The other is clamped circular plates. The comparisons show that the present method can always obtain accurate results for the completely free cases and one-end-fixed cylinders when compared to the 3-D Ritz method, and for the clamped circular plates when compared to the 3-D series method. Also, all the vibration modes can be revealed. Besides, the present formulation is simple, computer implementation and application is straightforward, and moreover, various types of displacement boundary conditions, such as simply supported conditions, can be easily imposed. This is very difficult for the Ritz method or the series method to achieve.

TABLE 8

Comparison of non-dimensional flexural vibration frequencies $\bar{\omega}$'s of the annular thick plates between the present, the 3-D Ritz (3DR), the 3-D Hutchinson's series method (3DH) and the 2-D Mindlin theory (2DM), with $a/h = 2{\cdot}5$, $b/a = 0{\cdot}5$ (mesh 10×4) and $a/h = 1$, $b/a = 0{\cdot}5$ (mesh 8×8)

				s			
a/h	*b/a*	*n*	Method	1	2	3	4
			Present	1·388	8·324	9·132	14·16
		0	3DR	1·388	8·321	9·127	14·133
			3DH	1·398	8·327	9·128	10·398
			2DM	1·388	8·324	9·370	10·593
		1	Present	1·944	8·041	8·537	8·949
			3DR	1·943	8·039	8·534	8·945
			3DH	1·950	8·040	8·539	8·946
			2DM	1·951	8·189	8·659	9·162
2·5	0·5	2	Present	0·6907	3·124	8·403	8·797
			3DR	0·691	3·123	8·400	8·793
			3DH	0·6901	3·127	8·404	8·794
			2DM	0·6923	3·142	8·461	8·964
		3	Present	1·681	4·452	8·812	8·990
			3DR	1·680	4·450	8·808	8·986
			3DM	1·682	4·453	8·990	10·234
			2DM	1·684	4·475	8·899	9·076
		0	Present	1·984	5·774	8·268	9·087
			3DR	1·984	5·772	8·258	9·084
			3DH	1·985	5·774	7·503	8·259
			2DM	1·985	6·720	7·547	10·010
		1	Present	1·999	3·930	5·841	7·708
			3DR	1·999	3·930	8·258	9·084
			3DH	2·000	3·930	5·841	6·401
			2DM	2·005	4·064	6·583	8·207
1	0·5	2	Present	1·039	2·846	5·173	6·159
			3DR	1·039	2·846	5·172	6·157
			3DH	1·040	2·846	5·173	6·159
			2DM	1·040	2·860	5·399	6·730
		3	Present	2·320	3·947	6·393	6·807
			3DR	2·320	3·946	6·392	6·805
			3DH	2·321	3·946	6·392	6·806
			2DM	2·324	3·971	6·749	7·311

Some observations from the present study may not be so familiar or may be beyond expectation. This merely shows the complex nature of the phenomena of plate vibration. In that case, due to the accuracy, simplicity and versatility of the present method, it should be a valuable alternative in the vibration analyses of annular and circular plates.

TABLE 9

Comparison of non-dimensional flexural vibration frequencies $\bar{\omega}$'s of the annular thick plates between the pesent, the 3-D Ritz (3DR) and the 3-D finite element method (3DF), with $a/h = 1{\cdot}7$, $b/a = 0{\cdot}1765$ (mesh 6×4)

			s				
	n	Method	1	2	3	4	5
Symmetric modes	0	Present	3·086	7·240	7·835	8·924	9·595
		3DR	3·0858	7·2372	7·8200	8·9145	9·5772
		3DF	3·0874	7·2457	7·8345	8·9372	9·7051
	1	Present	2·772	6·028	6·997	7·909	
		3DR	2·7717	6·0272	6·9938	7·8951	
		3DF	2·7778	6·0287	6·9986	7·9149	
	2	Present	1·973	4·052	6·386	7·791	8·138
		3DR	1·9684	4·0503	6·3799	7·7821	8·1282
		3DF	1·9776	4·0535	6·3915	7·8033	8·1379
Antisymmetric modes	0	Present	1·789	5·322	6·727	9·692	
		3DR	1·7884	5·3168	6·7194	9·6715	
		3DF	1·7899	5·3276	6·7422	9·7096	
	1	Present	2·908	5·572	6·039	6·150	
		3DR	2·9046	5·5678	6·0365	6·1431	
		3DF	2·9090	5·5755	6·0416	6·1547	
	2	Present	1·131	4·408	6·182	6·770	7·694
		3DR	1·1300	4·4052	6·1753	6·7662	7·6741
		3DF	1·1324	4·410	6·1907	6·7725	7·7279

TABLE 10

Comparison of non-dimensional flexural vibration frequencies $\bar{\omega}$'s of the solid circular cylinders with one end fixed between the present and the 3-D Ritz (3DR) methods, with $a/h = 0{\cdot}5$ (mesh 8×8) and $a/h = 0{\cdot}2$ (mesh 4×10)

		0·5		0·2	
n	*s*	Present	3DR	Present	3DR
0	1	1·286	1·286	0·511	0·511
	2	2·960	2·960	1·505	1·505
	3	3·170	3·169	2·371	2·370
	4	4·184	4·182	2·928	2·933
	5	4·300	4·298	2·987	3·009
1	1	0·5060	0·506	0·1060	0·106
	2	1·444	1·444	0·4785	0·478
	3	2·589	2·588	1·046	1·045
	4	2·854	2·854	1·597	1·601
	5	3·348	3·347	2·050	2·059
2	1	2·162	2·162	2·132	2·131
	2	2·519	2·519	2·343	2·343
	3	3·451	3·449	2·399	2·300
	4	3·761	3·760	2·608	2·609
	5	4·349	4·348	2·948	2·979

TABLE 10. *Continued*

		0·5		0·2	
n	*s*	Present	3DR	Present	3DR
3	1	3·258	3·258	3·258	3·255
	2	3·699	3·698	3·612	3·611
	3	4·292	4·290	3·627	3·626
	4	4·652	4·651	3·734	3·733
	5	5·356	5·355	3·941	3·964
4	1	4·282	4·281	4·299	4·295
	2	4·783	4·783	4·722	4·719
	3	5·206	5·204	4·740	4·738
	4	5·609	5·609	4·816	4·820
	5	6·148	6·147	4·965	4·978
5	1	5·275	5·271	5·317	5·316
	2	5·814	5·813	5·765	5·759
	3	6·152	6·150	5·790	5·785
	4	6·585	6·584	5·857	5·852
	5	6·984	6·983	5·979	5·983
6	1	6·251	6·243	6·328	6·333
	2	6·815	6·814	6·777	6·570
	3	7·105	7·102	6·806	6·764
	4	7·553	7·552	6·870	6·794
	5	7·885	7·886	6·979	6·859
7	1	7·218	7·204	7·341	7·349
	2	7·799	7·797	7·774	7·749
	3	8·057	8·054	7·806	7·781
	4	8·497	8·494	7·869	7·844
	5	8·846	8·848	7·969	7·946
8	1	8·181	8·163	8·356	8·364
	2	8·771	8·768	8·766	8·721
	3	9·007	9·002	8·800	8·755
	4	9·424	9·418	8·861	8·816
	5	9·843	9·847	8·957	8·909
9	1	9·143	9·126	9·375	9·378
	2	9·737	9·732	9·761	9·684
	3	9·956	9·949	9·795	9·719
	4	10·346	10·336	9·856	9·779
	5	10·826	10·837	9·947	9·873

TABLE 11

Comparison of non-dimensional flexural vibration frequencies of clamped circular plates for 3-D exact solution, 2-D Mindlin solution and the present solution (20×4 *mesh for* $a/h = 5$ *and* 10×4 *for* $a/h = 2{\cdot}5$)

	$a/h = 5$				$a/h = 2{\cdot}5$			
	1	2	3	4	1	2	3	4
Present	0·9102	2·993	5·644	8·557	1·487	4·099	7·055	9·992
3-D exact	0·909	2·987	5·634	8·541	1·482	4·086	7·032	9·965
2-DMindin	0·906	2·982	5·621	8·511	1·478	4·069	6·982	9·937

REFERENCES

1. A. W. LEISSA and J. SO 1995 *Journal of the Acoustical Society of America* **98**, 2122–2135. Comparisons of vibration frequencies for rods and beams from one-dimensional and three-dimensional analyses.
2. A. W. LEISSA and J. SO 1995 *Journal of the Acoustical Society of America* **98**, 2136–2141. Accurate vibration frequencies of circular cylinders from three-dimensional analysis.
3. J. SO and A. W. LEISSA 1998 *Journal of Sound and Vibration* **209**, 15–41. Three-dimensional vibrations of thick circular and annular plates.
4. J. R. HUTCHINSON 1979 *Journal of Applied Mechanics* **46**, 139–144. Axisymmetric flexural vibrations of a thick free circular plate.
5. J. R. HUTCHINSON 1984 *Journal of Applied Mechanics* **51**, 581–585. Vibrations of thick free circular plates, exact versus approximate solutions.
6. J. R. HUTCHINSON and S. A. EL-AZHARI 1986 *Refined Dynamical Theories of Beams, Plates, and Shells and Their Applications, Proceedings of the Euromech-Colloquium* **219**, 102–111. On the vibration of thick annular plates.
7. C. F. LIU and G. T. CHEN 1995 *International Journal of Mechanical Science* **37**, 861–871. A simple finite element analysis of axisymmetric vibration of annular and circular plates.
8. C. F. LIU and Y. T. LEE 1997 *Journal of Sound and Vibration* **208**, 47–54. Axisymmetric straining modes in the vibration of circular plates.
9. T. IRIE, G. YAMADA and S. AOMURA 1980 *Journal of Applied Mechanics* **47**, 652–655. Natural frequencies of Mindlin circular plates.
10. G. M. L. GLADWELL and D. K. VIJAY 1975 *Journal of Sound and Vibration* **42**, 387–397. Natural frequencies of free finite length circular cylinders.
11. J. SO 1993 *Ph.D. Dissertation, The Ohio State University*. Three-dimensional vibration analysis of elastic bodies of revolution. Table 3.28.
12. J. R. HUTCHINSON 1986 *Proceedings of the International Conference on vibration problems in Engineering, Xian, China, June* 19–22, 75–81. On the axisymmetric vibrations of thick clamped plates.

APPENDIX A

$$\begin{bmatrix} K^{11} & K^{12} & K^{13} \\ K^{21} & K^{22} & K^{23} \\ K^{31} & K^{32} & K^{33} \end{bmatrix} \{\ddot{U}\} + \begin{bmatrix} M^{11} & M^{12} & M^{13} \\ M^{21} & M^{22} & M^{23} \\ M^{31} & M^{32} & M^{33} \end{bmatrix} \{U\} = 0,$$

$$K_{ij}^{11} = \int_A \left[Q_{11} N_{i,r} N_{j,r} + Q_{13} \frac{1}{r} N_{i,r} N_j + Q_{13} \frac{1}{r} N_i N_{j,r} + Q_{33} \frac{1}{r^2} N_i N_j + Q_{55} n^2 \frac{1}{r^2} N_i N_j + Q_{66} N_{i,z} N_{j,z} \right] \pi r \, \mathrm{d}z \, \mathrm{d}r,$$

$$K_{ij}^{12} = \int_A \left[Q_{13} \frac{n}{r} N_{i,r} N_j + Q_{33} \frac{n}{r^2} N_i N_j - Q_{55} \left(\frac{n}{r} N_i N_{j,r} - \frac{n}{r^2} N_i N_j \right) \right] \pi r \, \mathrm{d}z \, \mathrm{d}r$$

$$= K_{ji}^{21}$$

$$K_{ij}^{13} = \int_A \left[Q_{12} N_{i,r} N_{j,z} + Q_{23} \frac{1}{r} N_i N_{j,z} + Q_{66} N_{i,z} N_{j,r} \right] \pi r \, \mathrm{d}z \, \mathrm{d}r = K_{ji}^{31}$$

$$K_{ij}^{22} = \int_A \left[Q_{33} \frac{n^2}{r^2} N_i N_j + Q_{44} N_{i,z} N_{j,z} + Q_{55} \left(N_{i,r} N_{j,r} - \frac{1}{r} N_{i,r} N_j \right. \right.$$

$$\left. \left. - \frac{1}{r} N_i N_{j,r} + \frac{1}{r^2} N_i N_j \right) \right] \pi r \, \mathrm{d}z \, \mathrm{d}r,$$

$$K_{ij}^{23} = \int_A \left[Q_{23} \frac{n}{r} N_i N_{j,z} - Q_{44} \frac{n}{r} N_{i,z} N_j \right] \pi r \, \mathrm{d}z \, \mathrm{d}r = K_{ji}^{32}$$

$$K_{ij}^{33} = \int_A \left[Q_{22} N_{i,z} N_{j,z} + Q_{44} \frac{n^2}{r^2} N_i N_j + Q_{66} N_{i,r} N_{j,r} \right] \pi r \, \mathrm{d}z \, \mathrm{d}r$$

$$M_{ij}^{11} = M_{ij}^{22} = M_{ij}^{33} = \int_A (\rho N_i N_j) \, \pi r \, \mathrm{d}z \, \mathrm{d}r,$$

$$M_{ij}^{12} = M_{ij}^{22} = M_{ij}^{13} = M_{ji}^{31} = M_{ij}^{23} = M_{ji}^{32} = 0,$$

where $i, j = 1$–m, and Q_{ij} are the stiffness coefficients from

$$\{\sigma\} = [Q_{ij}]\{\varepsilon\}.$$